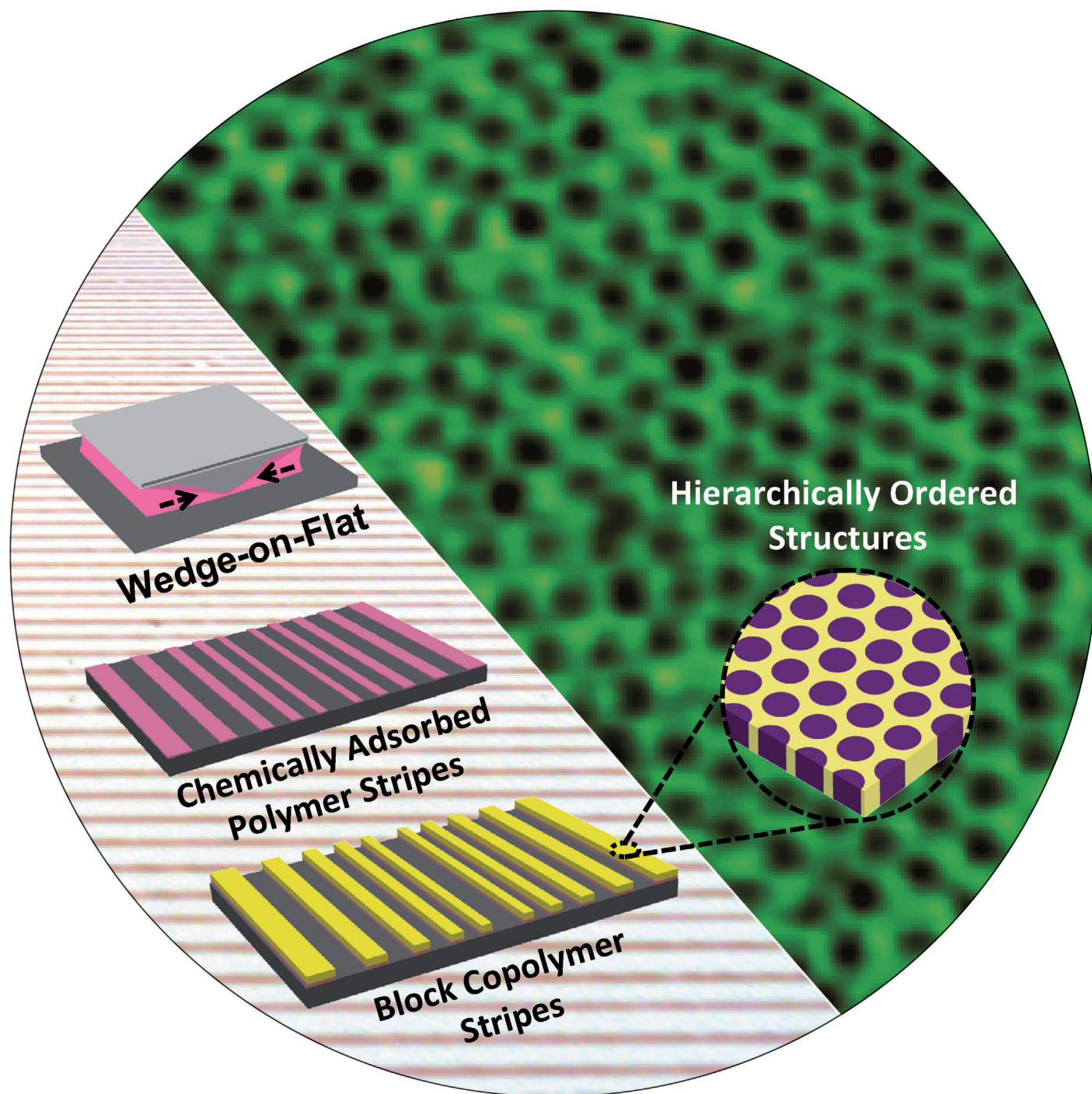**Hierarchically Ordered Structures**

An Unconventional Route to Hierarchically Ordered Block Copolymers on a Gradient Patterned Surface through Controlled Evaporative Self-Assembly**

*Myunghwan Byun, Wei Han, Bo Li, Xukai Xin, and Zhiqun Lin**

Wedge-on-Flat

Chemically Adsorbed Polymer Stripes

Block Copolymer Stripes

Hierarchically Ordered Structures

Pinned drying droplets that contain nonvolatile solutes (e.g., polymers, proteins, DNA, microspheres, nanoparticles, etc.) often give dissipative ring-like deposits (e.g., "coffee rings").[1] Structural evolution of these kinetically trapped surface patterns is primarily governed by the repetitive stick–slip (i.e., pinning–depinning) motion of the three-phase contact line of the drying droplet.[1,2] However, the formed structures are often stochastically distributed rather than uniform final deposits, largely because of the lack of control over the stick–slip motion and the presence of temperature-gradient-induced convective flux.[1,2] Therefore, a considerable challenge is the control of drying dynamics and creation of surface patterns of high regularity in a simple and cost-effective manner, thus eliminating the need for external-field and lithography techniques.[3] In this context, a few elegant preparative approaches have emerged, which give highly ordered structures and assemblies by enforcing the drying droplet to evaporate in restricted environments,[4] including "curve-on-flat" geometry,[4] two-plate geometry,[5] and cylindrical tube.[6] The use of these confined geometries provides an effective way to utilize the pinning–depinning process and minimize the possible convective instabilities, which in turn promotes the formation of uniform and well-controlled structures.

The self-assembly of nanoscale materials to hierarchically ordered structures offers new opportunities in the development of miniaturized optical, electronic, optoelectronic, and magnetic devices. Diblock copolymers that are composed of two chemically distinct chains covalently linked at one end are thermodynamically driven to self-assemble into a range of well-ordered nanoscopic domains (e.g., spheres, cylinders, double-gyroids, and lamellae) depending on the volume fraction of their components.[7] The domain size, which is dictated by the molecular weight of the block copolymers, is typically in a range of 10 to 100 nm. These morphologies can be employed as ideal templates and scaffolds for the fabrication of nanostructured materials and devices (e.g., magnetic storage media[8] and dye-sensitized solar cells[9]). The key in the use of block copolymers is the control over the orientation and lateral ordering of nanoscopic domains. In this regard, a variety of approaches have been developed to control the orientation and promote the lateral ordering of nanodomains by exploiting mechanical shearing,[10] external electric field,[11] temperature gradient,[12] solvent-vapor

annealing,[13] controlled interfacial interaction,[14] and topographically[15] or chemically patterned surfaces.[16] It is noteworthy that the use of topographically and chemically patterned surfaces to direct the self-assembly of block copolymers is reported to involve high processing and maintenance costs and requires an iterative, multistep procedure that makes the structure formation more complicated and less reliable.

Herein, we demonstrate a facile, yet robust strategy toward hierarchically ordered structures composed of diblock copolymers by utilizing two consecutive self-assembly processes at different length scales. Firstly, periodic stripe-like polymer patterns with a gradient in the thickness and width as well as the center-to-center distance between adjacent stripes were prepared at the microscopic scale by controlled evaporative self-assembly (CESA) of the polymer solution in a confined geometry consisting of a wedge-shaped lens situated on a flat Si substrate (i.e., a wedge-on-Si geometry); subsequently, polymer segments were chemically adsorbed on the Si substrate after extensive washing with solvent, forming ultrathin polymer stripes with a width gradient on the Si substrate. Secondly, when a diblock copolymer was spin-coated onto a Si substrate with stripes of an ultrathin polymer deposited onto it, a thin film of the diblock copolymer hierarchically self-assembled selectively on the polymer stripes; this behavior resulted from the synergy between solvent-vapor-assisted, unfavorable interfacial-interaction-driven destabilization of thin films of diblock copolymer on the chemically distinct surfaces (i.e., hydrophobic polymer stripes and hydrophilic Si substrate with 2 nm-thick native silicon oxide at the surface (referred to as the Si substrate)) at the microscopic scale and the solvent-vapor-promoted reconstruction of diblock copolymer domains at the nanometer scale. Remarkably, the fabrication of ultrathin polymer stripe patterns is simple, unconventional, and cost-effective, dispensing with the need for lithography techniques to prepare chemically patterned substrates, as in copious past work.

Poly(methyl methacrylate) (PMMA) with a number-average molecular weight of $534\ kg\,mol^{-1}$ and a polydiversity index (PDI; M_w/M_n) of 1.57 was selected for the formation of an ultrathin layer of PMMA stripes (Figure 1a, lower right panel). The solution of PMMA in toluene was confined in the gap between a wedge-like lens and a Si substrate (i.e., "wedge-on-Si" geometry; Figure 1a, upper left panel), thus forming a capillary-held microfluid (Figure 1a, upper middle panel). The dimension of the resulting patterns can be varied by tailoring the height of the wedge-shaped lens.[17] As toluene evaporated with the fastest evaporation speed from the capillary edge, PMMA was transported to the perimeter of the confined solution to pin the three-phase contact line (i.e., "stick").[18] As the deposition process progressed, the initial contact angle of the meniscus at the capillary edge gradually decreased to a critical value because of continuous evaporative loss of toluene, at which the depinning force (i.e., capillary force) became larger than the pinning force,[18] causing the contact line to move toward the wedge/Si contact center (i.e., "slip") and to stop at a new position, thereby leaving behind a stripe locally. Such consecutive, controlled "stick–slip" cycles of the receding contact line in the

[*] Dr. W. Han, B. Li, Dr. X. Xin, Prof. Z. Q. Lin
School of Materials Science and Engineering
Georgia Institute of Technology
Atlanta, GA 30332 (USA)
E-mail: zhiqun.lin@mse.gatech.edu
Homepage: http://nanofm.mse.gatech.edu/
Dr. M. Byun
Polymer Science and Engineering
University of Massachusetts Amherst
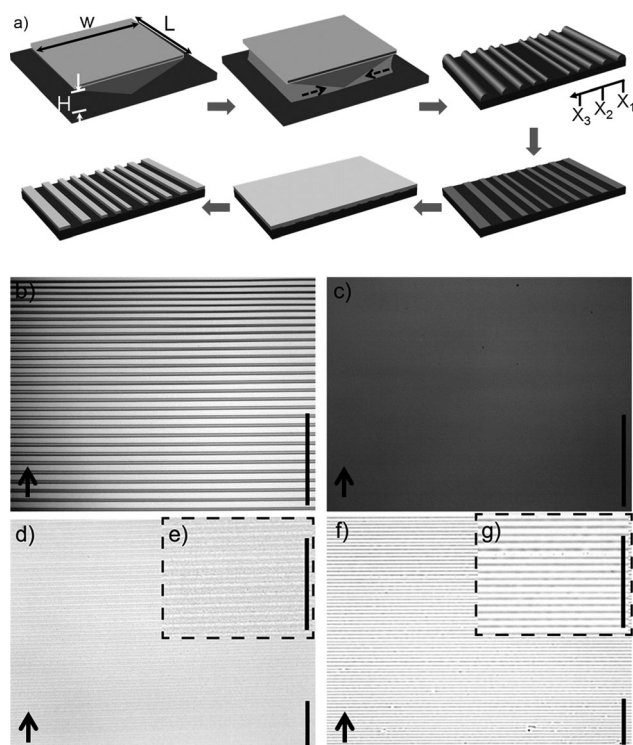Amherst, MA 01003 (USA)

Figure 1. a) Formation of hierarchically ordered PS-*b*-PEO stripes. Upper panels: gradient PMMA stripes were created by CESA of PMMA in toluene in the "wedge-on-Si" geometry. Lower panels: a thin PS-*b*-PEO film was spin-coated on the Si–PMMA. Preferential segregation of PS-*b*-PEO on ultrathin PMMA stripes resulted from vapor annealing with a benzene/water mixture. b) Representative optical micrograph of PMMA stripes. c) Chemically adsorbed ultrathin PMMA stripes after washing with acetone; the PMMA stripes appeared featureless under the optical microscope because of their ultralow thickness (≈ 5 nm). d) The spin-coated PS-*b*-PEO film on the Si–PMMA before mixed-solvent vapor annealing. e) Close-up optical micrograph of a small area in d. f) PS-*b*-PEO stripes segregated on ultrathin PMMA stripes after mixed-solvent vapor annealing. g) Close-up optical micrograph of the small area in f. b)–g) Scale bars = 100 μm. The arrows in b–d and f indicate the moving direction of the three-phase contact line.

symmetric "wedge-on-Si" geometry produced concentric stripes in a gradient arrangement globally, which was a direct consequence of the competition between the linear pinning force and the nonlinear capillary force[18] governed by the shape of the wedge (Figure 1 a, upper right panel).[17] Locally, the resulting surface patterns appeared as periodic straight stripes (Figure 1 b). The height of PMMA stripes ranged from (133 ± 8) nm at the outermost region X_1 to (97 ± 6) nm at the intermediate region X_2 and to (45 ± 3) nm at the innermost region X_3 as measured by atomic-force microscopy (AFM, data not shown), where X_n is the distance to the wedge/Si contact center (Figure 1 a, upper right panel).

These gradient PMMA stripes on the Si substrate were then vigorously washed with acetone. Quite intriguingly, an ultrathin layer of PMMA was found to be chemically adsorbed on the Si substrate (Figure 1 a, lower right panel, and Figure 1 c). The adsorbed PMMA film was ultrathin (below 5 nm). As a result, alternating hydrophobic ultrathin PMMA stripes and hydrophilic Si substrate surfaces were

obtained in an unconventional manner at low cost. Obviously, when a droplet of water was placed on an Si substrate with ultrathin PMMA stripes deposited onto it (i.e., Si–PMMA), the three-phase contact line of water was evenly undulated because of the different wettabilities of hydrophilic native silicon oxide and hydrophobic PMMA stripes (Figure 2 a). Furthermore, X-ray photoelectron spectroscopy (XPS) measurements on PMMA stripes before and after extensive acetone washing clearly displayed the presence of a hydrocarbon peak (C−C and C−H) at a binding energy of 285.0 eV and a weak carbonyl peak at 288.8 eV from PMMA after washing (Figure 2 b), suggesting the anchoring of ultrathin PMMA stripes.
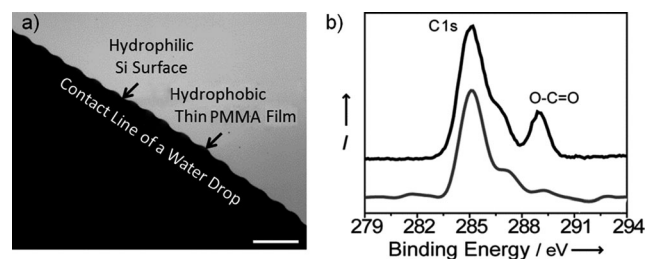

Figure 2. a) Optical micrograph of the three-phase contact line of a water droplet on the Si–PMMA. The undulation of the contact line is clearly evident. Scale bar = 50 μm. b) XPS spectra in the C1s region of PMMA stripes on the Si substrate before (upper curve) and after (lower curve) vigorous washing with acetone. The hydrocarbon peak (C−C and C−H) at a binding energy of 285.0 eV and the weak carbonyl peak at 288.8 eV (O−C=O) from PMMA were still present after treatment with acetone.

The formation of chemically adsorbed ultrathin PMMA stripes on the Si substrate can be rationalized as follows. During the evaporation process, the adsorption of PMMA on the Si substrate may arise from the hydrogen bonding between the silanol group of silicon oxide and the carbonyl group of PMMA.[19] The hydroxy group of silicon oxide surface may also be capable of hydrolyzing the ester bond on the side chain of PMMA to produce a carboxylate side chain, which bonds ionically with the silicon oxide surface.[19] After washing with acetone, the PMMA chains that were weakly deposited onto this chemically anchored PMMA were thoroughly removed, leaving behind a chemically anchored ultrathin PMMA layer.

The resulting ultrathin PMMA stripes with a width gradient were then exploited as the chemically patterned surface, onto which a solution of an asymmetric diblock copolymer, polystyrene-*block*-poly(ethylene oxide) (PS-*b*-PEO), in dimethylformamide (DMF, $c = 10$ mg mL^{-1}) was spin-coated (Figure 1 a, lower middle panel). The average molecular weight (MW) of PS-*b*-PEO was 25.4 kg mol^{-1}, and the weight fraction of PS (MW = 19 kg mol^{-1}) and PEO (MW = 6.4 kg mol^{-1}) are approximately 0.75 and 0.25, respectively. Figure 1 d shows an optical micrograph of a thin PS-*b*-PEO film spin-coated on gradient ultrathin PMMA stripes, which were chemically anchored on the Si substrate as noted above. Subsequently, the thin PS-*b*-PEO film was exposed to the vapor of a mixture of benzene/water (4:1) for 1 h in

a sealed vessel at room temperature. Quite intriguingly, at the microscopic scale, as the benzene/water-vapor annealing progressed, the thin PS-*b*-PEO film migrated from the hydrophilic Si substrate and preferentially segregated onto ultrathin PMMA stripes (i.e., dewetting-driven contraction of continuous thin PS-*b*-PEO films; see Figure 1e, and Figure S1 in the Supporting Information). The AFM measurements showed that the dimensions of PS-*b*-PEO stripes, that is, the center-to-center distance between adjacent stripes (λ_{c-c}) and the stripe width (w), were gradually decreased with an increasing proximity to the wedge/Si contact center, from $\lambda_{c-c} = (6.0 \pm 0.3)$ µm and $w = (3.1 \pm 0.2)$ µm at the outermost region X_1, to $\lambda_{c-c} = (4.7 \pm 0.2)$ µm and $w = (2.2 \pm 0.1)$ µm at the intermediate region X_2, and to $\lambda_{c-c} = (3.9 \pm 0.2)$ µm and $w = (1.8 \pm 0.2)$ µm at the innermost region X_3. It is worth noting that these dimensions were identical to original PMMA stripes that were formed by controlled evaporative self-assembly (Figure 1b, upper right panel). The height of deposited PS-*b*-PEO stripes ($\approx (25 \pm 2)$ nm) was uniform over the entire deposition area; this was approximately commensurate with the periodic length scale of the neighboring PEO nanocylinders (≈ 30 nm).[20]

We now turn our attention to address qualitatively why thin PS-*b*-PEO films migrated from (i.e., dewetted) the Si substrate (i.e., Si stripes in the present study) to ultrathin PMMA stripes, forming PS-*b*-PEO patterns on the ultrathin PMMA stripes only. In principle, the PS blocks tend to segregate to the air surface, forming a PS-rich layer because of the lower surface energy of PS compared with PEO (i.e., $\gamma_{PS} = (35.1 \pm 0.1)$ mJ m^{-2} and $\gamma_{PEO} = (40.3 \pm 0.2)$ mJ m^{-2}), and PEO blocks would preferentially interact with the Si substrate through intermolecular hydrogen bonding between the ether oxygen atoms of PEO segments and hydroxy groups of the Si substrate.[20] Thus, the dewetting of cylinder-forming PS-*b*-PEO on the Si substrate (i.e., Si stripes) can be attributed to the high volume fraction of PS blocks (75 % by volume) in PS-*b*-PEO. It has been shown both experimentally and theoretically that a thin PS film is unstable on the Si substrate with 2 nm thick native silicon oxide at the surface, because of a positive value of the Hamaker constant (A), which signifies the interfacial interaction between the polymer and the substrate.[21] In particular, unfavorable interfacial-interaction-driven destabilization of thin PS-*b*-PEO films on Si stripes (i.e., dewetting), that is, the local segregation of PS-*b*-PEO on the ultrathin PMMA stripes (i.e., wetting) can be understood by taking into account the spreading coefficient, $S = \gamma_2 - (\gamma_1 + \gamma_{1/2})$, and the effective Hamaker constant for the van der Waals (vdW) interaction,[22] where γ_1 and γ_2 are the surface tension of the top layer (1) and the bottom layer (2), respectively; $\gamma_{1/2}$ is the interfacial tension between layer 1 and layer 2. If the effective Hamaker constant (A_{eff}) is positive, the film is likely to be destabilized (i.e., dewetting), whereas if A_{eff} is negative, the film would be stable for $S > 0$ (i.e., wetting) and metastable for $S < 0$, depending strongly on the thickness of the film. The spreading coefficients for PS-*b*-PEO/SiO$_2$ (PS-*b*-PEO on SiO$_2$) and PS-*b*-PEO/PMMA (PS-*b*-PEO on PMMA) were calculated to be positive, i.e., $S_{SiO_2/PS-b-PEO} = 11.8$ mJ m^{-2} and $S_{PMMA/PS-b-PEO} = 15.1$ mJ m^{-2}.[23] The A_{eff} can be approximated by

$$A_{eff} \approx \frac{3}{4} kT \left(\frac{\varepsilon_s - \varepsilon_f}{\varepsilon_s + \varepsilon_f} \right) \left(\frac{\varepsilon_v - \varepsilon_f}{\varepsilon_v + \varepsilon_f} \right)$$
$$+ \frac{3 h v_e}{8\sqrt{2}} \frac{\left(n_s^2 - n_f^2 \right) \left(n_v^2 - n_f^2 \right)}{\left(n_s^2 - n_f^2 \right)^{1/2} \left(n_v^2 - n_f^2 \right)^{1/2} \left[\left(n_s^2 - n_f^2 \right)^{1/2} + \left(n_v^2 - n_f^2 \right)^{1/2} \right]}$$

(1)

in which ε_i is the dielectric constant, n_i are the refractive indices ($i = s$ (substrate), f (film), and v (vapor of a mixture of benzene/water), respectively), and $h v_e \approx 20 \times 10^{-19}$ J is the electronic UV absorption energy. The A_{eff} was estimated as follows: $A_{SiO_2/PS-b-PEO/(benzene/water)} = 3.9 \times 10^{-20}$ J and $A_{PMMA/PS-b-PEO/(benzene/water)} = 1.1 \times 10^{-20}$ J. Interestingly, both $A_{SiO_2/PS-b-PEO/(benzene/water)}$ and $A_{PMMA/PS-b-PEO/(benzene\&water)}$ are positive, thus reflecting that PS-*b*-PEO was unstable on either the Si substrate or the PMMA stripes during the solvent-vapor annealing process. However, compared with the Si substrate, because of a relatively lower $A_{PMMA/PS-b-PEO/(benzene\&water)}$ than $A_{SiO_2/PS-b-PEO/(benzene/water)}$, the thin PS-*b*-PEO film tended to destabilize from the Si substrate and segregate to the PMMA stripes. It is not surprising that as the mixed-solvent-vapor annealing was carried out over a period of 1 h, the segregated PS-*b*-PEO stripes became destabilized and broke into randomly distributed droplet-like structures because of Rayleigh instability to minimize the surface energy (Figure S2).[24]

Remarkably, in conjunction with the dewetting of a thin PS-*b*-PEO film on the Si substrate at the microscopic scale (as discussed above), the lateral surface reconstruction of PS-*b*-PEO was also promoted at the nanometer scale during the benzene/water-vapor annealing (Figure 3), as a result of markedly different vapor pressure between benzene and water (i.e., 14 kPa for benzene and 2.4 kPa for water).[20] For the PS-*b*-PEO diblock copolymer, benzene is a neutral
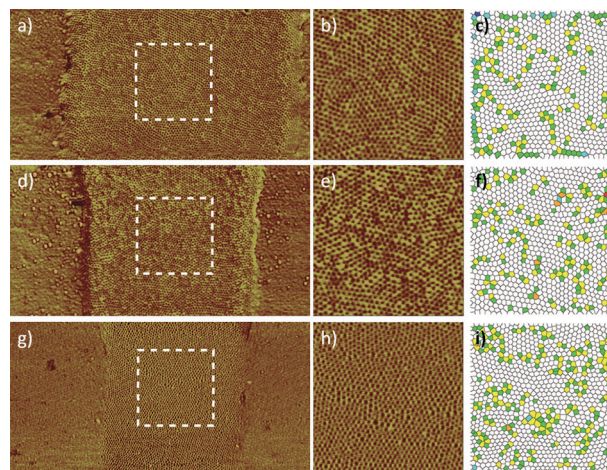

Figure 3. Representative AFM phase images of PS-*b*-PEO stripes on ultrathin PMMA stripes in three different regions: a) outermost region (X_1), d) intermediate region (X_2) and g) innermost region (X_3). Image sizes = 2×4 µm². b, e, and h) close-up AFM phase images, corresponding to the dashed white squares marked in a, d, and g. Image sizes = 1×1 µm². c, f, and i) Corresponding Voronoi diagrams. Colored lattices are defects. Sixth-order rate was almost 70 % in these three images.

solvent with similar affinity for both PS and PEO blocks because of similar polymer–solvent interaction parameters for PS/benzene and PEO/benzene ($\chi_{PS/benzene} = 0.34$ and $\chi_{PEO/benzene} = 0.43$).[25] By contrast, water is a selective solvent for the PEO block as $\chi_{PEO/water}$ (1.26) is smaller than $\chi_{PS/water}$ (4.40).[25] Hexagonally ordered arrays of vertical nanocylinders were observed after exposing a thin PS-*b*-PEO film to the benzene/water vapor for 1 h right after preswelling of the film under water vapor for 1 h; the latter was conducted to prevent a rapid dewetting of the swollen thin PS-*b*-PEO film because of higher vapor pressure of benzene during the annealing process.[20] As reported in previous studies,[25] a thin PS-*b*-PEO film that is exposed to the vapor of neat benzene tends to align PEO nanocylinders predominantly parallel to the substrate, because of a slight difference in the degree of swelling (benzene vapor is slightly preferential to PS block rather than PEO block as $\chi_{PS-benzene} = 0.34 < \chi_{PEO-benzene} = 0.43$) and very similar values of their surface tensions ($\gamma_{PS} = (35.1 \pm 0.1)$ mJ m^{-2} and $\gamma_{PEO} = (40.3 \pm 0.2)$ mJ m^{-2}). The addition of water at the volume fraction ratio of benzene/water = 4:1 may mitigate the PS selectivity upon exposure to the mixed-solvent vapor, thus leading to the transition of parallel nanocylinders to vertical nanocylinders as softer PEO blocks were primarily swollen by water.[20] The close-up AFM phase images (Figure 3 b, e, and h) clearly show hexagonally ordered PS-*b*-PEO nanostructures that are confined on the gradient ultrathin PMMA stripes. Thus, hierarchically ordered structures composed of PS-*b*-PEO were crafted through two consecutive self-assembly processes at different length scales, namely, 1) gradient concentric ultrathin PMMA stripes at the microscopic scale produced by the CESA in the "wedge-on-Si" geometry, followed by the removal of weakly adsorbed PMMA, and 2) spontaneous self-assembly and reconstruction of PS-*b*-PEO diblock copolymer at the nanometer scale on gradient micrometer-sized PMMA stripes. Hexagonal ordering of PEO nanocylinders with approximately 70% sixth-order rate was achieved over the entire deposition area (see Voronoi diagrams in Figure 3 c,f, and i, in which red-, blue-, green-, and orange-colored lattices were defects without sixth-order rate).

To confirm the vertical orientation of PEO nanocylinders from the air interface to the substrate, AFM imaging was performed, examining the bottom side of the resulting PS-*b*-PEO patterns originally in contact with the ultrathin PMMA stripes, from which the PEO cylindrical nanodomains were also found to align perpendicularly to the substrate (Figure S3). We note that the precise control over the film thickness can be readily realized by simply varying either the concentration of the PS-*b*-PEO solution or the speed of spin-coating (Figure S4; formation of (50 ± 2) nm-thick stripes).

In summary, we demonstrated a particularly versatile approach to craft hierarchically ordered structures composed of diblock copolymers on gradient chemically patterned surfaces by utilizing two consecutive self-assembly processes at different length scales. Notably, ultrathin, chemically adsorbed polymer stripes were prepared in a simple, unconventional, and remarkably controllable manner at low cost, eliminating the need for costly and multistep lithography techniques. These hierarchically ordered structures may find

potential applications in optics, electronics, optoelectronics with tunable functionalities, and desirable spatial arrangements. Additionally, they may serve as a useful template to selectively incorporate inorganic nanoparticles, and a platform to study cell adhesion and motility, and neuron guidance.

Experimental Section

Wedge-on-Si geometry: A wedge lens made of aluminum and a Si wafer with a 2 nm-thick native silicon oxide layer were used as the upper and lower surfaces, respectively, the wedge-on-Si geometry. The area at the sides of the wedge and the wedge height were 1×1 cm^2 and 1000 μm, respectively. The Si substrate was cleaned using a mixture of sulfuric acid and NOCHROMIX, and then vigorously rinsed with deionized water and blown dry with N$_2$. The wedge-on-Si geometry was placed in a sealed vessel to minimize possible air convection and to maintain constant temperature during the controlled evaporative self-assembly (CESA) process.

Materials, surface modification, and characterization, thin-film preparation, solvent-vapor annealing: PMMA ($M_n = 534$ kg mol^{-1}, PDI = 1.57, Sigma Aldrich) was dissolved in toluene (c = 0.25 mg mL^{-1}). XPS measurement was performed to give additional information on the chemically adsorbed PMMA before and after acetone treatment. PS-*b*-PEO ($M_n = 25.4$ kg mol^{-1}, vol% of PS = 0.75, PDI = 1.05; Polymer Sources Inc.) was dissolved in dimethylformamide (DMF) at two concentrations (10 and 20 mg mL^{-1}). Thin PS-*b*-PEO films were spin-coated on the Si substrate with ultrathin PMMA stripes deposited onto it (i.e., Si-PMMA), and subsequently vapor-annealed with a mixture of benzene/water (4:1) for 1 h right after preswelling with water for 1 h.

Characterization of surface morphologies: The PMMA stripes formed on the flat Si substrate and PS-*b*-PEO films were thoroughly examined by optical microscopy (OM; BX51 optical microscope in reflection mode (Olympus)) and atomic-force microscopy (AFM; Dimension 3100 scanning-force microscope in tapping mode (Digital Instrument)) before and after acetone treatment. BS-tap 300 tips (Budget Sensors) with spring constants ranging from 20 to 75 N m^{-1} were used as scanning probes.

[1] R. D. Deegan, O. Bakajin, T. F. Dupont, G. Huber, S. R. Nagel, T. A. Witten, *Nature* **1997**, *389*, 827–829.

[2] E. Adachi, A. S. Dimitrov, K. Nagayama, *Langmuir* **1995**, *11*, 1057–1060.

[3] a) J. R. Friend, L. Y. Yeo, D. R. Arifin, A. Mechler, *Nanotechnology* **2008**, *19*, 145301; b) T. P. Bigioni, X. M. Lin, T. T. Nguyen, E. I. Corwin, T. A. Witten, H. M. Jaeger, *Nat. Mater.* **2006**, *5*, 265–270; c) M. Gleiche, L. F. Chi, H. Fuchs, *Nature* **2000**, *403*, 173–175; d) B. P. Khanal, E. R. Zubarev, *Angew. Chem.* **2007**, *119*, 2245–2248; *Angew. Chem. Int. Ed.* **2007**, *46*, 2195–2198.

[4] a) W. Han, Z. Q. Lin, *Angew. Chem.* **2012**, *124*, 1566–1579; *Angew. Chem. Int. Ed.* **2012**, *51*, 1534–1546; b) W. Han, M. Byun, B. Li, X. Pang, Z. Q. Lin, *Angew. Chem.* **2012**, *124*, 12756–12760; *Angew. Chem. Int. Ed.* **2012**, *51*, 12588–12592.

[5] a) B. H. Kim, D. O. Shin, S. J. Jeong, C. M. Koo, S. C. Jeon, W. J. Hwang, S. Lee, M. G. Lee, S. O. Kim, *Adv. Mater.* **2008**, *20*, 2303–2307; b) H. S. Kim, C. H. Lee, P. K. Sudeep, T. Emrick, A. J.

Crosby, *Adv. Mater.* **2010**, *22*, 4600–4604; c) H. Yabu, M. Shimomura, *Adv. Funct. Mater.* **2005**, *15*, 575–581.

[6] M. Abkarian, J. Nunes, H. A. Stone, *J. Am. Chem. Soc.* **2004**, *126*, 5978–5979.

[7] C. J. Hawker, T. P. Russell, *MRS Bull.* **2005**, *30*, 952–966.

[8] T. Thurn-Albrecht, J. Schotter, C. A. Kastle, N. Emley, T. Shibauchi, L. Krusin-Elbaum, K. Guarini, C. T. Black, M. T. Tuominen, T. P. Russell, *Science* **2000**, *290*, 2126–2129.

[9] E. J. W. Crossland, M. Nedelcu, C. Ducati, S. Ludwigs, M. A. Hillmyer, U. Steiner, H. J. Snaith, *Nano Lett.* **2009**, *9*, 2813–2819.

[10] D. E. Angelescu, J. H. Waller, D. H. Adamson, P. Deshpande, S. Y. Chou, R. A. Register, P. M. Chaikin, *Adv. Mater.* **2004**, *16*, 1736–1740.

[11] T. Thurn-Albrecht, J. DeRouchey, T. P. Russell, H. M. Jaeger, *Macromolecules* **2000**, *33*, 3250–3253.

[12] J. Bodycomb, Y. Funaki, K. Kimishima, T. Hashimoto, *Macromolecules* **1999**, *32*, 2075–2077.

[13] a) S. H. Kim, M. J. Misner, T. Xu, M. Kimura, T. P. Russell, *Adv. Mater.* **2004**, *16*, 226–231; b) S. Ludwigs, A. Boker, A. Voronov, N. Rehse, R. Magerle, G. Krausch, *Nat. Mater.* **2003**, *2*, 744–747.

[14] P. Mansky, Y. Liu, E. Huang, T. P. Russell, C. J. Hawker, *Science* **1997**, *275*, 1458–1460.

[15] a) I. Bita, J. K. W. Yang, Y. S. Jung, C. A. Ross, E. L. Thomas, K. K. Berggren, *Science* **2008**, *321*, 939–943; b) R. A. Segalman, H. Yokoyama, E. J. Kramer, *Adv. Mater.* **2001**, *13*, 1152–1155.

[16] a) S. O. Kim, H. H. Solak, M. P. Stoykovich, N. J. Ferrier, J. J. de Pablo, P. F. Nealey, *Nature* **2003**, *424*, 411–414; b) L. Rockford, Y. Liu, P. Mansky, T. P. Russell, M. Yoon, S. G. J. Mochrie, *Phys. Rev. Lett.* **1999**, *82*, 2602–2605.

[17] a) M. Byun, N. B. Bowden, Z. Q. Lin, *Nano Lett.* **2010**, *10*, 3111–3117; b) M. Byun, W. Han, F. Qiu, N. B. Bowden, Z. Q. Lin, *Small* **2010**, *6*, 2250–2255.

[18] J. Xu, J. F. Xia, S. W. Hong, Z. Q. Lin, F. Qiu, Y. L. Yang, *Phys. Rev. Lett.* **2006**, *96*, 066104.

[19] J. F. Watts, S. R. Leadley, J. E. Castle, C. J. Blomfield, *Langmuir* **2000**, *16*, 2292–2300.

[20] S. Park, D. H. Lee, J. Xu, B. Kim, S. W. Hong, U. Jeong, T. Xu, T. P. Russell, *Science* **2009**, *323*, 1030–1033.

[21] S. W. Hong, J. F. Xia, Z. Q. Lin, *Adv. Mater.* **2007**, *19*, 1413–1417.

[22] a) G. G. Baralia, C. Filiatre, B. Nysten, A. M. Jonas, *Adv. Mater.* **2007**, *19*, 4453–4459; b) J. Israelachvili, *Intermolecular & Surface Forces*, Academic Press, New York, **1992**.

[23] S. H. Lee, P. J. Yoo, S. J. Kwon, H. H. Lee, *J. Chem. Phys.* **2004**, *121*, 4346–4351.

[24] M. D. Morariu, E. Schaffer, U. Steiner, *Phys. Rev. Lett.* **2004**, *92*, 156102.

[25] J. Brandrup, E. H. Immergut, *Polymer Handbook*, Wiley, New York, **1989**.